We are IntechOpen, the world's leading publisher of Open Access books Built by scientists, for scientists

4,800
Open access books available

122,000
International authors and editors

135M
Downloads

Our authors are among the

154
Countries delivered to

TOP 1%
most cited scientists

12.2%
Contributors from top 500 universities

CLARIVATE ANALYTICS BOOK CITATION INDEX INDEXED

WEB OF SCIENCE™

Selection of our books indexed in the Book Citation Index in Web of Science™ Core Collection (BKCI)

Interested in publishing with us?
Contact book.department@intechopen.com

Numbers displayed above are based on latest data collected.
For more information visit www.intechopen.com

2

Neutron Diffraction Measurements for Residual Stresses in AL-6XN Stainless Steel Welded Beams

Xiaohua Cheng[1,*], Henry J. Prask[2,3], Thomas Gnaeupel-Herold[2,3], Vladimir Luzin[4,**] and John W. Fisher[5]

[1]*New Jersey Department of Transportation, Trenton, NJ*
[2]*NIST Center for Neutron Research, Gaithersburg, MD*
[3]*University of Maryland, College Park, MD*
[4]*Australian Nuclear Science & Technology Organization*
[5]*ATLSS Research Center, Lehigh University, Bethlehem, PA*
[1,2,3,5]*USA*
[4]*Australia*

1. Introduction

The primary objective of the current study was to quantify the magnitude and distribution of residual stresses in various welded details in non-magnetic super-austenitic AL-6XN stainless steel I-beams through saw cutting and neutron diffraction methods. The welded details included transverse groove welds and simulated bulkhead attachment welded details, both of which duplicated details in previous fatigue test specimens [Fisher et al., 2001; Cheng et al., 2003a]. It was expected that the results of a study of residual stresses could be used to analyze the effect of residual stresses on fatigue strength. This Chapter presents a description of specimen materials, specimen preparation, neutron diffraction measurement plan, method and results.

2. Background, materials and testing methods

2.1 Background

Residual stresses are introduced into structural steel components during manufacturing and fabricating processes. For welded structures, weld process, weld sequence, component size and setup restraint, temperature or cooling rate difference, and material composition and properties are primary factors that affect residual stresses. Residual stresses can have significant impact on ultimate strength, stability, fatigue strength and toughness depending on their magnitude and distribution with respect to stresses from applied external loads and dead loads.

---

[*] formerly with ATLSS Reserach Center, Lehigh University, USA
[**] formerly with NIST Center for Neutron Research, USA

Since a loaded structure is subjected to both internal residual stress and stress from externally applied loads, the resultant stress should be their superposition [Cheng et al., 2003b]. Tensile residual stresses can cancel out compressive loading stresses that are favourable for fatigue strength. Once the resultant stress exceeds the yield stress, plastic flow occurs in a mild steel material (such as carbon-manganese (C-Mn) steel). Consequently, stress range is one controlling factor for fatigue strength rather than the maximum applied stress. Combined with applied stresses, for example, the residual stress distribution along a lateral weld in a beam may indicate where a fatigue crack first develops, whereas the through-thickness residual stress gradient may affect fatigue crack propagation. Therefore, studies of the magnitude and distribution of residual stresses are needed.

The AL-6XN steel in this study is a non-magnetic super-austenitic stainless steel that has potential application in ship structures which use the advanced double hull (ADH) concept due to its high strength, superior crevice corrosion resistance, low magnetic signature, excellent fracture toughness and great ductility. It is a stable, single-phase austenitic (face-centered cubic) alloy. Standard tension and compression tests showed that the material is isotropic and homogeneous. The stress-strain relationship is approximately bilinear without the yielding flow plateau that C-Mn mild steel has. Because of its greater nickel content, AL-6XN steel has about a 20% higher coefficient of thermal expansion than carbon steel (15.20 μm/m/°K vs. 12.06 μm/m/°K or 8.44 μ in./in./°F vs. 6.7 μ in./in./°F), but only 1/4 the thermal conductivity of carbon steel (12.9 W/(m·K) vs. 51.9 W/(m·K) or 89.5 Btu·in./(ft²·hr.·°F) vs. 360 Btu·in./(ft²·hr·°F)) [INCO, 1964; Lamb, 1999; Dudt, 2000]. Consequently, residual stresses in welded components of AL-6XN steel may be more localized and greater than those observed in carbon steels. A well-understood residual stress state is desired as a part of material characterization to evaluate fatigue strength.

The magnitude of residual stresses introduced into a material is associated with the yield strength and ultimate tensile strength of the material. For large welded structural members, the higher the material yield strength, the greater the residual stresses. For AL-6XN steel, the minimum specified 0.2% offset yield strength and tensile strength are 45 ksi (310 MPa) and 95~100 ksi (655~690 MPa), respectively, depending on the plate thickness for the AL-6XN alloy [Rolled Alloys, 1997; Lamb, 1999]. The coupon test by Lehigh University [Lu *et al.*, 2002] and the mill report provided by Rolled Alloys showed that the 0.2% offset uniaxial nominal yield strength and ultimate tensile strength were 48.1~55.8 ksi (332~385 MPa) and 108~111 ksi (745~766 MPa), respectively, for ½" (12.7 mm) thick flange plates, and 50.9~62 ksi (351~428 MPa) and 105.1~113 ksi (725~780 MPa), respectively, for 3/8" (9.5 mm) thick web plates.

For comparison, the Inconel 625 filler metal used for welding the specimens in the current study typically has a yield strength of 72.5~85 ksi (500~590 Mpa) and a tensile strength of 114~116 ksi (790~800 Mpa). The mechanical properties of the IN625 filler metal (ERNiCrMo3) should comply with AWS A5.14 and ASME SFA5.14.

The measurements in this study focused on the magnitude and on lateral and through-thickness distributions of residual stresses in the beam's longitudinal direction, which was the same as the fatigue stress direction, for a transverse groove weld and an attachment fillet weld detail in AL-6XN stainless steel I-beams tested in the fatigue study program [Fisher, et al., 2001].

2.2 Types of residual stresses

There are three types of residual stresses: 1) Macroscopic residual stress, which extends over several grains and usually many more. It is in self-equilibrium and can be relieved elastically when the member is cut or sectioned; 2) Structural micro-stress, occurring in one grain or part of a grain. It can occur between different phases or between particles, and strongly depends on micro-structure characteristics, such as grain size and grain orientation. It arises because of different thermal contractions in different crystallographic directions and is not diminished by cutting the sample. It is a grain interaction stress that promotes deleterious processes, such as stress corrosion cracking and hydride cracking; 3) Intra-granular stress, even more microscopic, ranging over several atomic distances within a grain and equilibrated over this small part of a grain. In this study, only the macroscopic residual stress was addressed.

Macroscopic residual stresses produced by welding can be decomposed into local welding stress and global welding stress [Campus, 1954]. Local weld stresses are developed in every case, even when welded pieces are small and completely free. These stresses are localized near the weld, most concentrated in the heat affected zone (HAZ), and decrease rapidly away from the weld. When welded pieces are restrained, that is, the thermal deformations are restrained, stresses will be produced everywhere in the pieces, which are called global welding stresses. Local and global stresses exist together and are in equilibrium. Once restraints are removed, the elastic part of global stresses should disappear, but plastic deformation due to global stress yielding and local stresses remain. In most cases, it is hard to separate them in a large welded assembly. Nevertheless, understanding the concept of local and global stresses is important and helpful in explaining many engineering fractures and phenomena in large welded structures.

2.3 Measuring techniques and selection of measuring methods

Since Mathar's pioneering work using a hole drilling method in 1934, various techniques for measuring residual stresses have been developed and applied in industry and research laboratories [e.g. SEM, 1996; HYTEC, 2001; Ritchie et al., 1987; Sherman, 1969]. These techniques include (1) hole drilling; (2) layer removal; (3) sectioning; (4) X-ray diffraction; (5) neutron diffraction; (6) ultrasonic; and (7) electro-magnetic methods. Since each measuring method is limited to a certain use and precision, no one method is ideal to measure a large-scale specimen with a rather complex geometry, such as welded beams with attachments. In most cases, two or more methods are combined to meet industrial needs and achieve a required precision.

In this study, two measurement methods, saw cutting (sectioning) and neutron diffraction, were selected and employed. Neutron diffraction measurements were conducted on groove weld and bulkhead attachment details in fabricated AL-6XN stainless steel beams because of advantages over traditional mechanical methods: it is non-destructive; it has triaxial through-thickness measurement capacity; it has flexibility with respect to sample geometry and material properties; and the measurement is localized in a region. Segment cutting from large-scale welded beams was needed because of limitations on the size of the neutron diffraction equipment, as discussed in Section 4 below.

3. Test specimens and measurement plan

Two welded I-beams of AL-6XN steel identical to those for fatigue tests [Fisher et al., 2001] were used for residual stress measurements, one with transverse groove welds in flange and web (Figure 1), and the other with one AL-6XN steel attachment detail welded to a flange (Figure 2). The weld conditions and sequence can be found in the report [Cheng et al., 2003a]. Residual stresses were measured at three weld details in these two beams: the transverse groove weld in the first beam, and the longitudinal flange-web weld and attachment fillet weld in the second beam. Table 1 summarizes the measurement plan for the two beams, including saw cut segment, sectioning and neutron diffraction methods. The results from different methods are superposed to obtain the final results [Cheng et al., 2003a]. However, only the neutron diffraction method and results are presented in this Chapter.

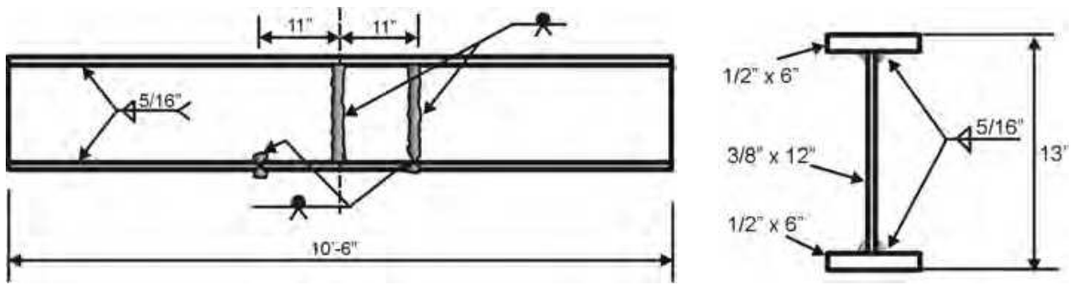

Fig. 1. Groove welded beam for residual stress measurement (unit: inch; 1 inch=25.4mm)

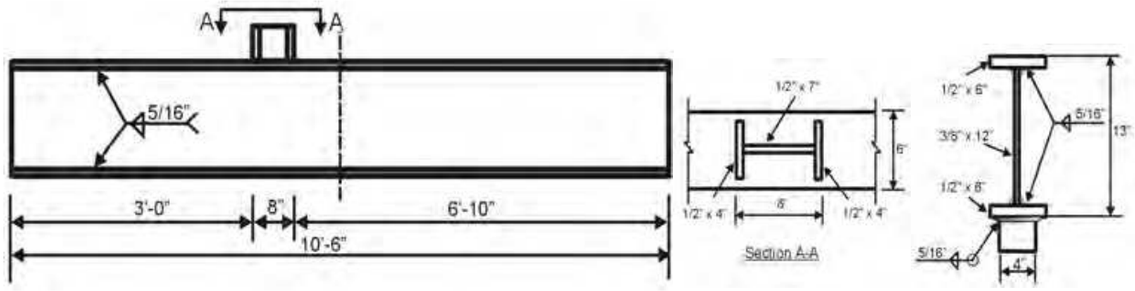

Fig. 2. Attachment Beam for Residual Stress Measurement (unit: inch; 1 inch=25.4mm)

Welded Beam	Weld Detail	Measuring Method	
Groove Welded Beam	Groove Weld	Two Steps	Saw Cut Segment
			Neutron Diffraction
Attachemnt Beam	Attachment Fillet Welds	Two Steps	Saw Cut Segment
			Neutron Diffraction
	Longitudinal Fillet Weld	-	Sectioning

Table 1. Summary of measurement plan

3.1 Saw cut segments from welded beams

Figures 3 and 4 show the locations, dimensions and most relevant portion of test segments for neutron diffraction meaurements for the groove-weld and attachment-weld details, respectively. Figure 5 shows a segment saw cut for the attachment beam. The stress release

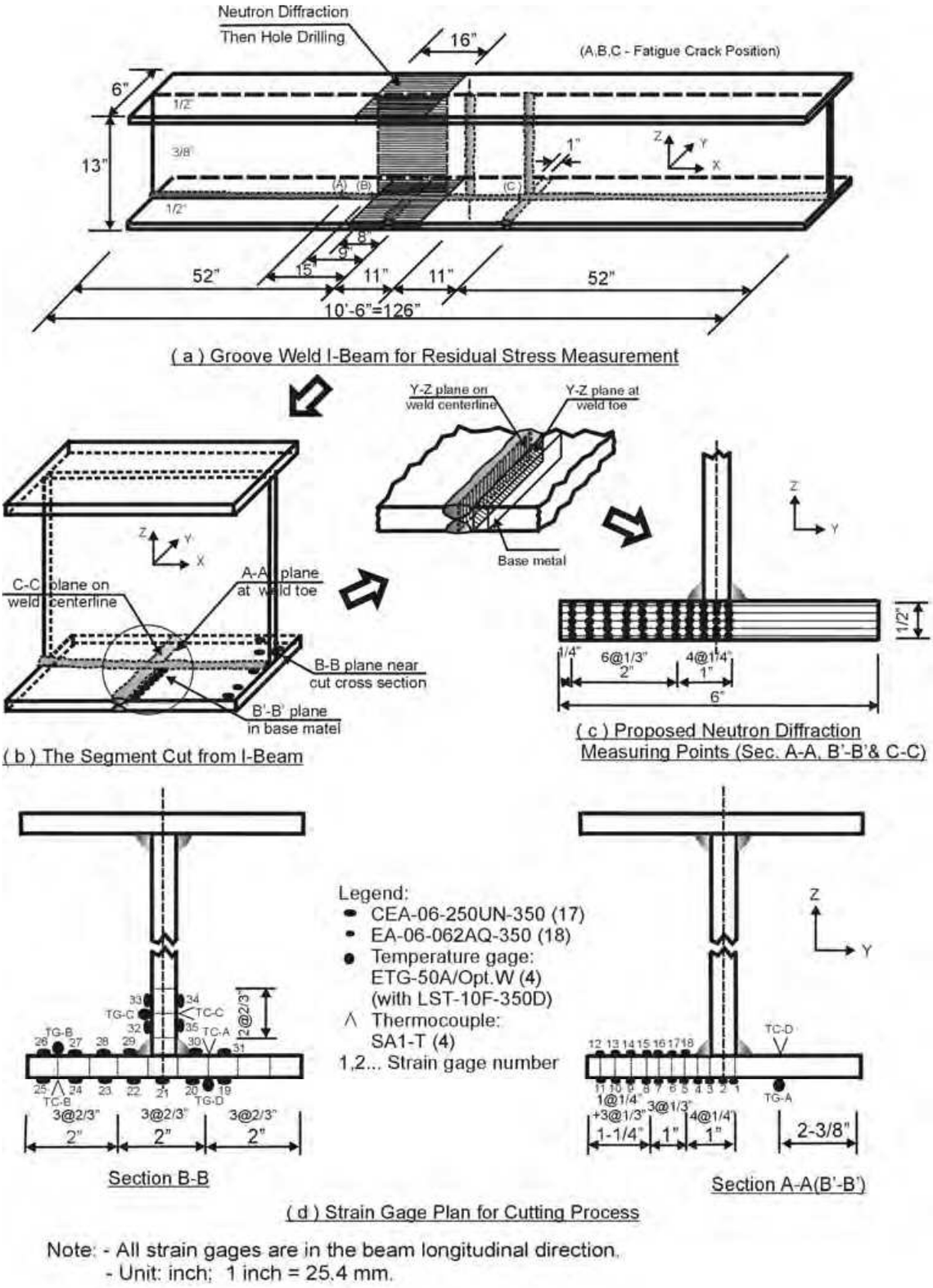

Fig. 3. Two-step residual stress measurement of groove welded beam

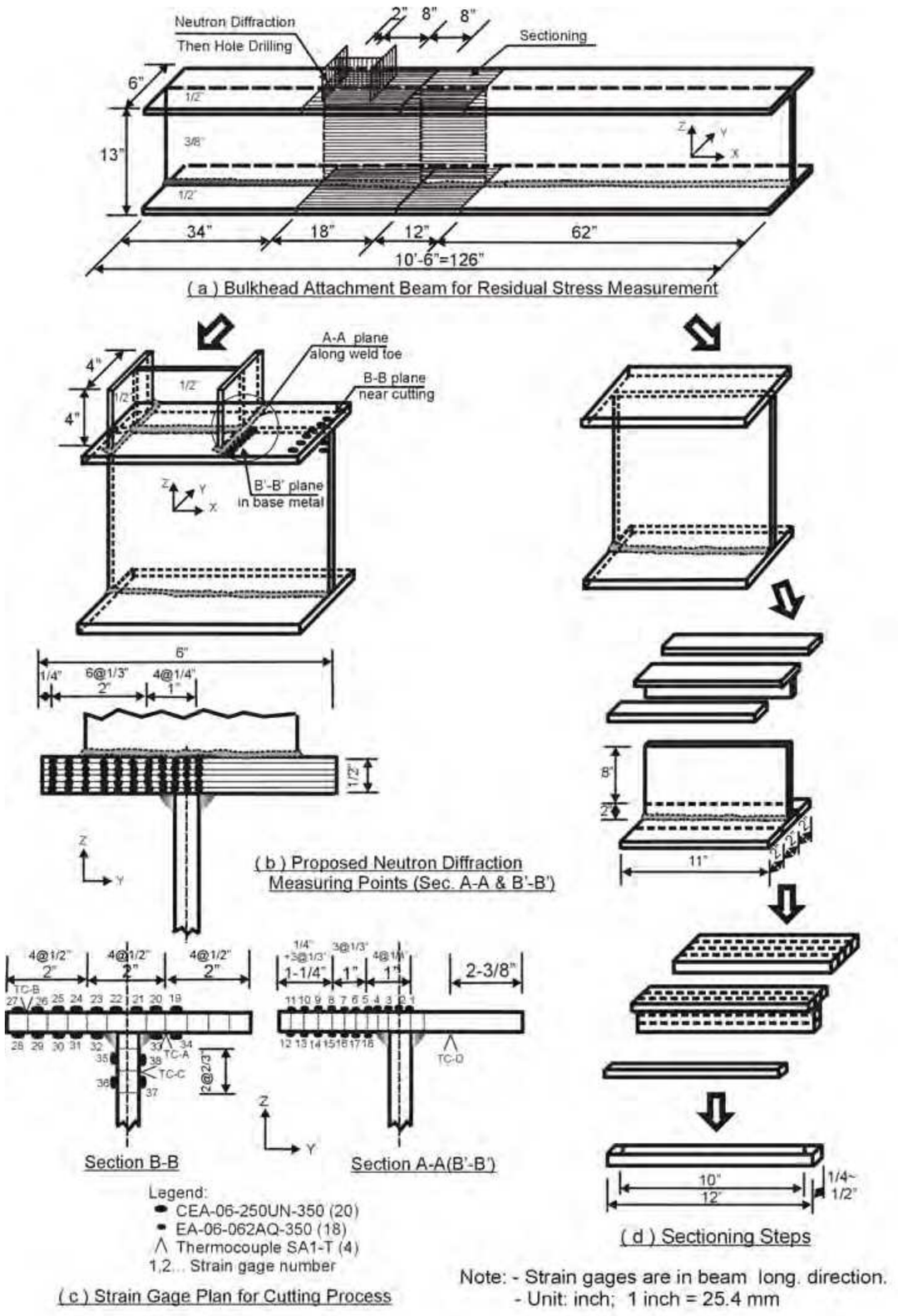

Fig. 4. Two-step residual stress measurement of attachment beam

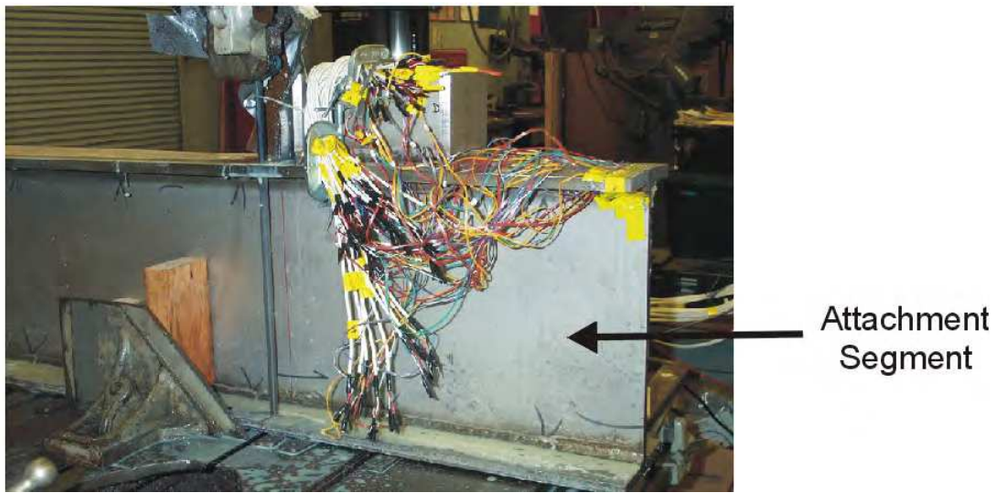

Fig. 5. Saw cut for attachment beam

due to saw cutting was recorded by strain gages. Strain gages were mounted near the weld toe and adjacent to the cross section of saw cut, shown in Figure 3(d) and Figure 4(c), to measure the residual stress release due to saw cutting. More details for saw cut procedure, data collection of stress release, as well as the segment of longitudinal weld used with the sectioning method can be found in the report [Cheng et al., 2003a; Tebedge et al., 1973; 1969].

3.2 Segments for neutron diffraction measurement

After saw cutting and stress release analysis, the remaining segments for groove weld and attachment weld details were shipped to NIST for neutron diffraction measurements. The groove weld segment was 406 mm long, 152 mm wide and 330 mm deep (16 x 6 x 13 inches) (Figure 3(a)), while the attachment segment was 457 mm (18 in.) long (Figure 4(a)).

4. Neutron diffraction measuring method

4.1 Principle

Neutron diffraction measurement is a physical and non-destructive measuring process that evaluates residual strain/stress through measuring the change in crystallographic lattice spacing (d-spacing) and utilizing the relationship between crystallographic parameters and residual stresses. The technique utilizes the penetrating power of neutrons that is ~10^3 greater than X-rays in the diffraction wave-length regime to map subsurface triaxial stress distributions [e.g. NATO ASI Series, 1992; Prask et al., 2001; SEM, 1996]. The crystallographic lattice spacing is quantified by observing the intensity of the diffracted neutron beam. As shown in Figure 6 the lattice spacing in a certain orientation, d_{hkl}, can be obtained by the Bragg Law where λ is neutron beam wavelength and θ is the Bragg angle. Consequently, residual strain locked in the material can be calculated from Eq.1 by knowing the change of lattice spacing before (d_0) and after (d) residual stress was introduced.

$$\varepsilon_{hkl} = \frac{d_{hkl} - d^0_{hkl}}{d^0_{hkl}} \tag{1}$$

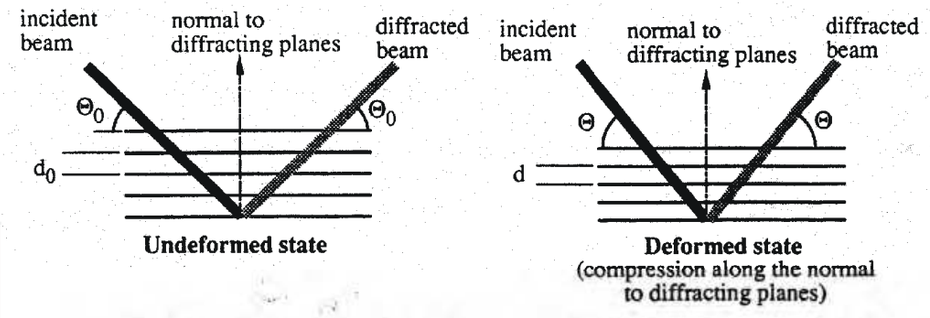

(a) Neutron Diffraction Measurement for Different Lattice Spacing

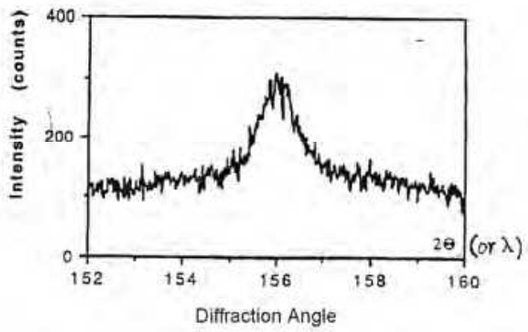

Bragg Law:

$$n\underline{\lambda} = 2d_{hkl}\sin\underline{\theta} \qquad (n=1)$$

(b) Neutron Diffraction Observation and Bragg Law for Calculating Lattice Spacing

Fig. 6. Principle of neutron diffraction measurement [SEM, 1996]

Two coordinate systems are utilized (Figure 7). One is the specimen-fixed coordinates (X, Y, Z) and the other is a laboratory coordinate system (L_i) corresponding to the scattering configuration. The measured lattice spacing is an average value over a number of grains covered in the neutron beam gage volume which is of the order of mm^3. The residual stress result is a kind of macro-stress that can be described by tensor components ε_{ij} or σ_{ij} in the specimen coordinate system (X,Y,Z). For a neutron beam with wavevector Q(ϕ,ψ) on the axis L_3, the measured strain along L_3 in the laboratory system ($\varepsilon_{\phi\varphi}'$ or ε_{33}') that satisfies the Bragg Law, can be converted to stresses in specimen-fixed axes as shown in Section 5.2. Eq.2 shows how the measured strains in the laboratory system are related to the the actual strains in the sample:

$$\varepsilon'_{\varphi,\psi} = [\varepsilon_{xx}\cos^2\phi + \varepsilon_{yy}\sin^2\phi + \varepsilon_{xy}\sin 2\phi]\sin^2\psi +$$

$$+\varepsilon_{xz}\cos\phi\sin 2\psi + \varepsilon_{yz}\sin\phi\sin 2\psi + \varepsilon_{zz}\cos^2\psi \qquad (2)$$

The superscript ′ indicates strain in the laboratory coordinate system. Measuring strains at a point for at least six distinct (ϕ,ψ) orientations yields all six residual strain components at that point. These strains can be converted to strains in the specimen axes, including the beam longitudinal direction (fatigue stress direction in fatigue tests). Further details for neutron diffraction can be found elsewhere [Society for Experimental Mechanics (SEM) 1996; NATO 1992; Prask *et al.* 1996].

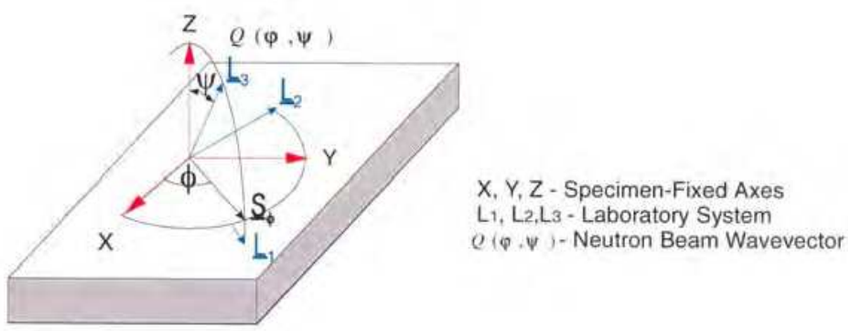

Fig. 7. Two coordinate systems for neutron diffraction measurement

4.2 Neutron diffraction measurement for segments

Due to limited space on the neutron diffraction table, from each 3.2 m (10.5 ft) long beam, a segment was cut to fit the instrument's X-Y-Z table and keep the residual stress relaxation at the location of interest as small as possible.

Segment saw cutting was done at Lehigh University (Bethlehem, PA), and neutron diffraction measurements were conducted at the NIST Center for Neutron Research (Gaithersburg, MD). At NIST, residual stress measurements on the segments were focused on weld toe (A-A plane), base metal (B'-B' plane on the centerline of mounted strain gages) and weld metal (C-C plane) (Figures 3(b), 4(b)). In each plane, measurements included both points near the surface for distribution along the weld bead and points through the plate thickness. To reduce the total number of measurement points, it was assumed that the residual stress distribution was symmetrical about the beam web centerline. The measurement point mesh (resolution) depends on the expected residual stress gradient and gage volume of the neutron beam, shown in Figure 3(c) for groove weld and in Figure 4(b) for attachment fillet weld. After evaluating the grain size of virgin AL-6XN material and needed path lengths, a gage volume 3 x 3 x 3 mm^3 was chosen.

4.3 Test setup and measurement procedure at NIST facilities

The neutron diffraction measurements were made with a constant wavelength from a steady state reactor. The diffractometer (BT-8) is specially designed and well-suited for strain measurement of various shape-complexities and compositions [NIST, 2011]. Figure 8 shows a schematic of the measurement method. The (311) reflection of face-centered cubic (FCC) iron (γ-iron) with corresponding d-spacing about 1.095 Å (1Å=0.1nm (10^{-7}mm)) was chosen for the strain measurements. A wavelength λ=1.518 Å was used at a scattering angles of 88°. A position sensitive detector (PSD) centered at 88˚ covered an angular range from 84˚ to 91˚, which corresponds to 1.133 to 1.064 Å in d-spacing scale. Figure 9 shows the groove weld segment placed on the X-Y-Z translator table of the neutron diffraction equipment. The incident beam is from the left tube, while the aperture of the neutron detector in the back of the photo receives the diffracted (scattered) beam. The X-Y-Z table is under computer control with a specimen weight limit of 50 kg (110 lbs). The part of the greatest interest for the groove weld and attachment fillet weld, is shown by the circles in Figure 3 and Figure 4, respectively.

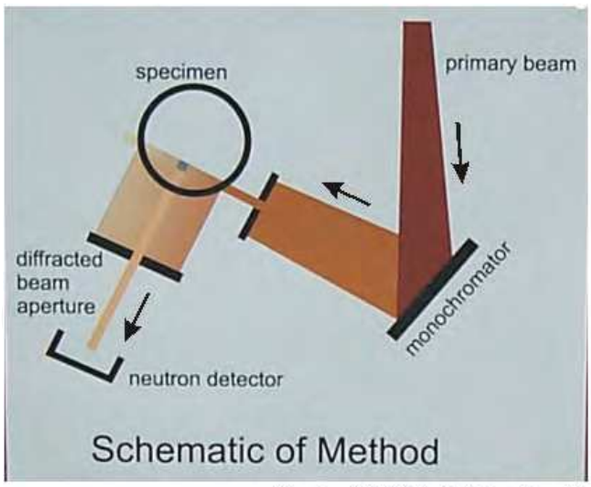

Fig. 8. Schematic of neutron diffraction method

Fig. 9. Groove welded beam segment on neutron diffraction X-Y-Z translator table

For a given specimen, d_0-spacing varies across the specimen (from base metal to weld metal). To measure the d_0-spacing, a smaller piece with base metal and weld cut from a similar AL-6XN beam was used to provide a stress-free reference sample. From this piece, one columnar shape coupon was cut from the base metal region and three were cut from the weld metal [NIST, 2003]. The d_0-spacing measurements were made on these coupons with gage volume of 2 mm x 2 mm x 2 mm. The average values of d_0 ($d_0(x)$, $d_0(y)$, $d_0(z)$) in three different directions were used for strain calculation (Eq.1).

5. Results from neutron diffraction measurements for groove weld segment

The groove weld joint was approximately in the middle of the segment specimen. It was a one-side GMAW weld without bevels on each plate and was back gouged. Groove welds were first made to connect two plates forming a flange or web member, then two welded flanges and a web were welded by longitudinal welds to assemble an I-beam. The maximum width of the weld zone was about 20mm (25/32 in.), as seen in Figure 10.

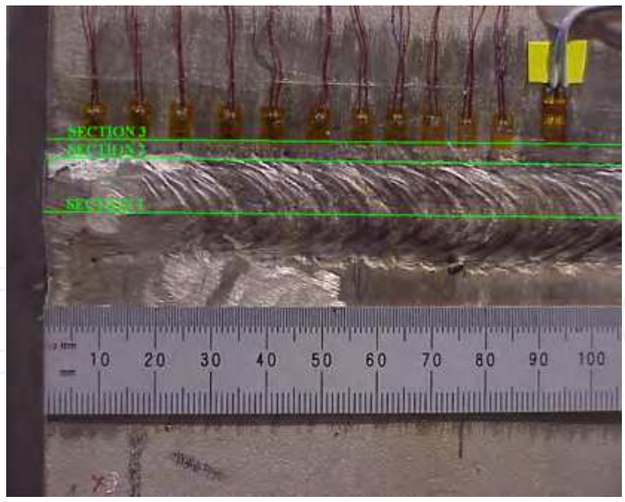

Fig. 10. Groove weld area on flange of the groove welded beam (outer surface)

5.1 Measurement locations

As shown in Figure 11, neutron diffraction measurements were made at three different sections: at the weld toe (Section 2 or A-A plane in Figure 3(b)), weld centerline (Section 1 or C-C plane) and base metal (Section 3 or B′-B′ plane). At each section the measuring mesh was basically the same (Figure 11). Measurement of the (311) lattice spacing was made in four different directions for each location. The specimen-fixed coordinate system is X-Y-Z, shown in Figure 11. The X-component which is in the fatigue stress direction was obtained by measuring two oblique directions corresponding to ϕ =±41.7° (≈±42°) with respect to the X-axis (see Figure 7) in the X-Y plane because of geometric complexity and high neutron beam absorption. The nominal increment step in flange thickness (Z) direction was 2.25 mm (0.09 in.) and was dictated mainly by spatial resolution of the experimental setup of the neutron diffractometer. The mesh in the Y direction (along the groove weld bead) was the same as the strain gage spacing used during segment saw cutting, so that straightforward superposition of the results from the neutron diffraction measurements and the saw cutting measurement could be made.

5.2 Measurement results

From the change of measured lattice spacing d and d_0 (d_0 & d: before and after residual stress is introduced), strain was obtained at each measurement point using Eq.1. The original strain data for the weld metal, weld toe and base metal are shown in Figures 12(a), 12(b), and 12(c), respectively. Figure 13 shows the stresses at the weld toe converted from the obtained strains using Eq.3:

$$\sigma_{ij} = \frac{1}{\frac{1}{2}S_2(hkl)}\{\varepsilon_{ij} - \delta_{ij}\frac{S_1(hkl)}{\frac{1}{2}S_2(hkl) + 3S_1(hkl)}(\varepsilon_{xx} + \varepsilon_{yy} + \varepsilon_{zz})\} \tag{3}$$

where i, j denotes one of the X, Y, Z specimen-fixed coordinates; S_1 and S_2 are the two diffraction elastic constants; $S_1(311)$ = 6.64 TPa^{-1} and $1/2S_2(311)$ = -1.61 TPa^{-1} for AL-6XN

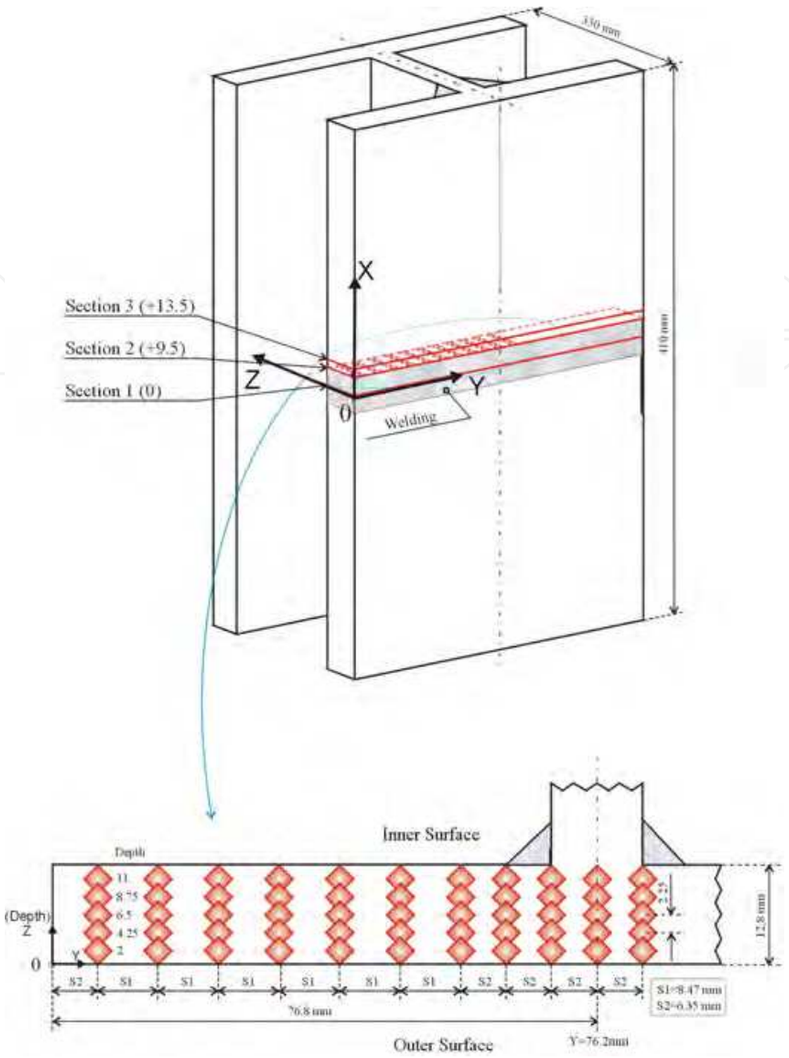

Fig. 11. Schematic measurement grid in specimen-fixed coordinate system (X-Y-Z), for groove weld segment (Unit: mm; 25.4mm=1 inch; gage volume 3x3x3mm^3)

stainless steel. S_1 and S_2 were obtained using Young's modulus, E=1.97x10^5 MPa (28,550 x10 ksi) and Poisson's ratio, v=0.33, for AL-6XN stainless steel, and single crystal constants given in [Danilkin et al., 2001]. δ_{ij} is the Kronecker delta which equals one when $i = j$ and zero when $i \neq j$. The uncertainties on measured d-spacings are determined by counting statistics and least-squares fits to the Gaussian peak shapes. The uncertainties on strains and stresses are determined from standard error propagation methods. Additional systematic errors are discussed below. Figure 14 shows the stress contour plots (for the weld toe) from the same measurements.

At Section 2 (at the weld toe), the measurement near the outer surface (nominal depth Z=2mm) included both base metal and weld metal, and would be sensitive to the weld content. The presence of weld metal complicated the measurement because of the different grain size and d_0 value for the base metal and weld metal. This was most obvious near the flange tip (Y=6.3mm) where more weld metal was included due to the start/stop end of

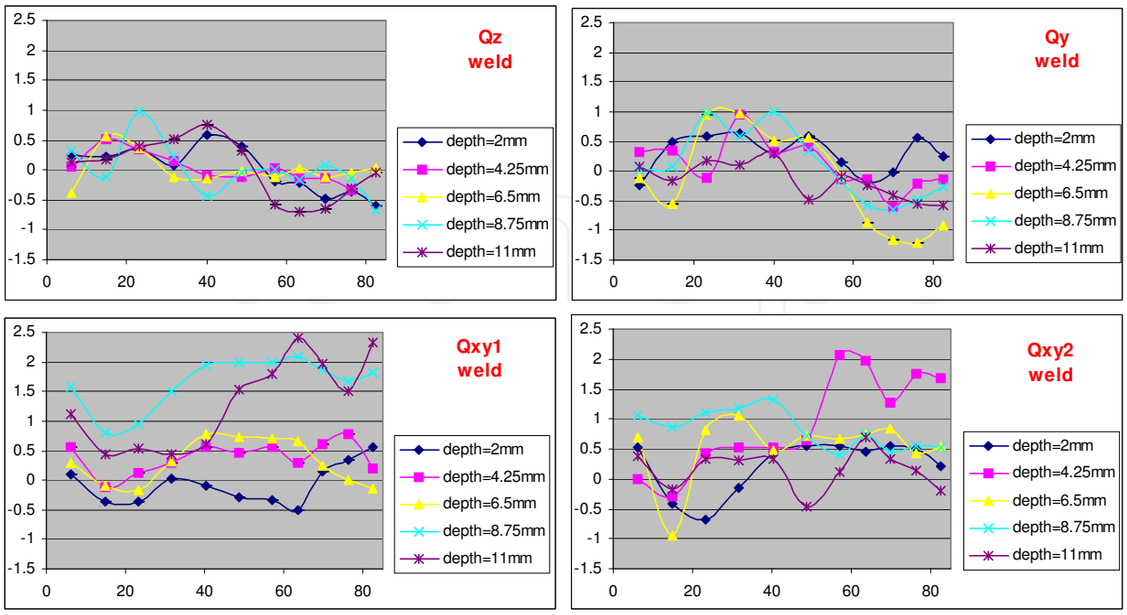

Fig. 12(a). Original strain data (x10^{3}μ) for weld centerline in groove-weld segment, (Qxy1 and Qxy2 correspond to φ = ±42°; counting-statistic uncertainties are typically about ±0.035; abscissa is Y-distance from flange edge (mm; beam centerline is 76.8mm)

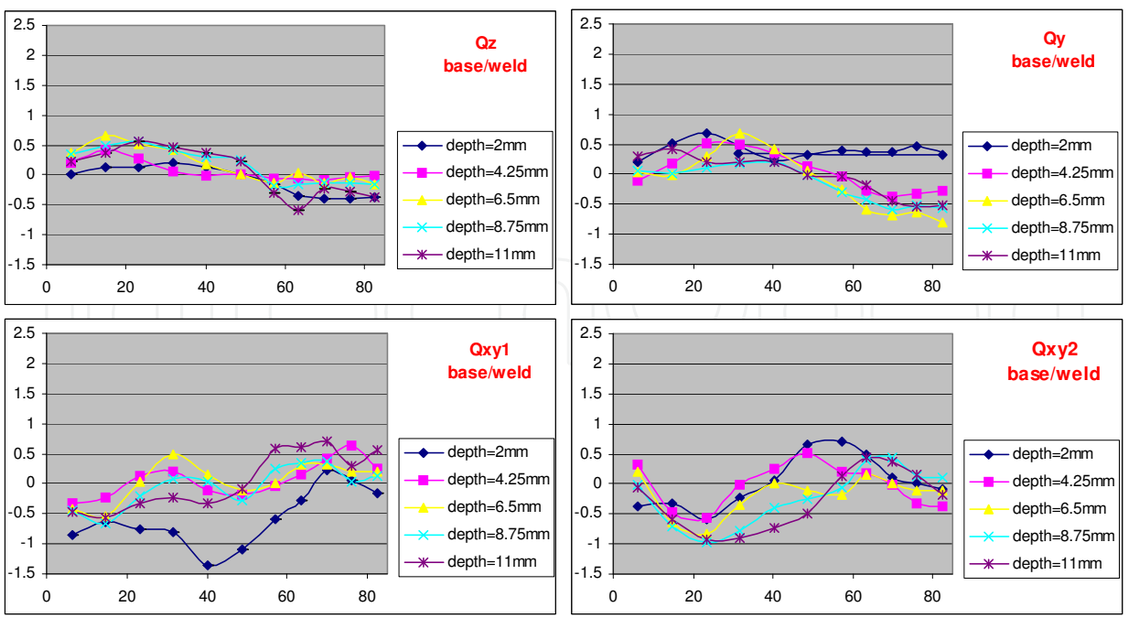

Fig. 12(b). Original strain data (x10^3 micro-strain) for weld toe in groove-weld segment, (Qxy1 and Qxy2 correspond to φ = ±42°; counting-statistic uncertainties are typically about ±0.035; abscissa is Y-distance from flange edge (mm; beam centerline is 76.8mm)

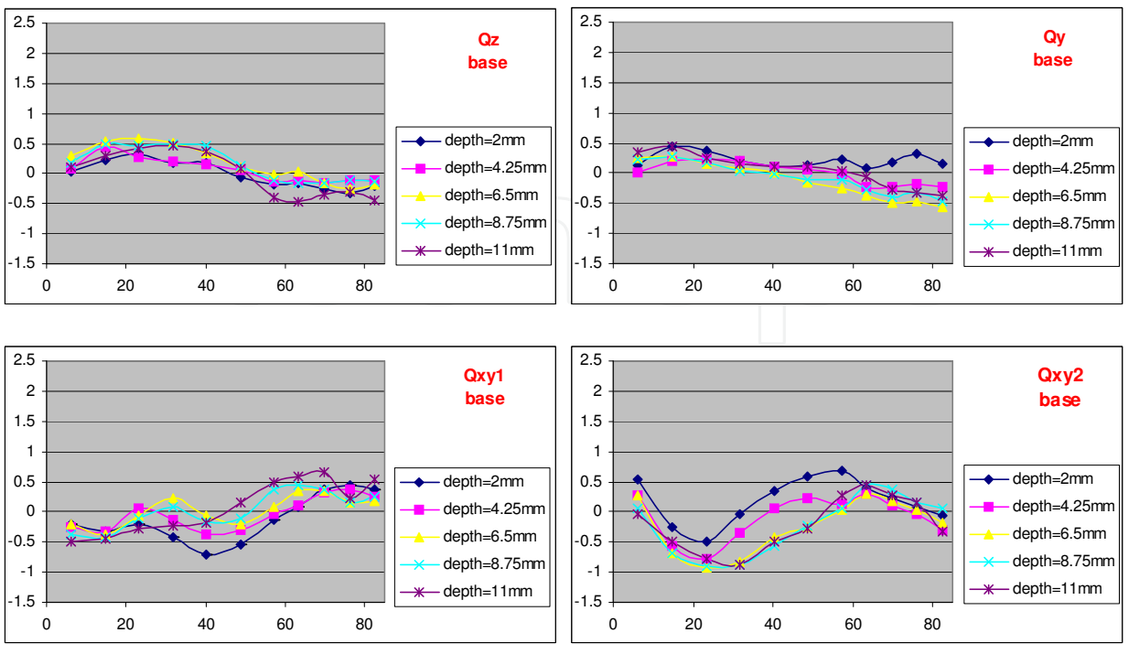

Fig. 12(c). Original strain data (x10^3 micro-strain) for base metal in groove-weld segment (Qxy1 and Qxy2 correspond to φ = ±42°); counting- statistic uncertainties are typically about ±0.035; abscissa is Y-distance from flange edge (mm; beam centerline is 76.8mm)

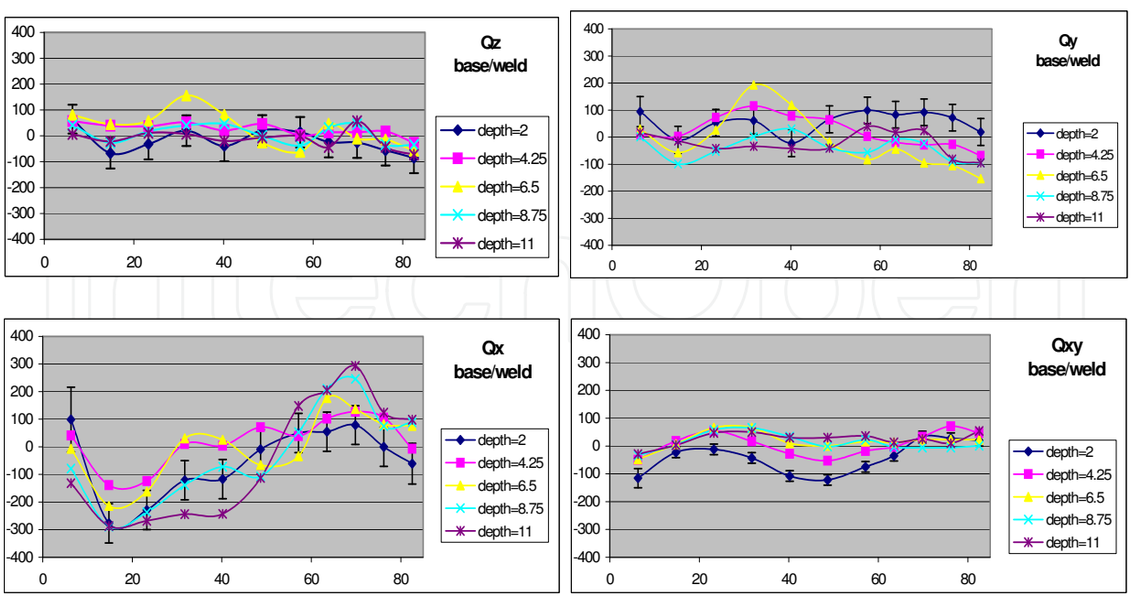

Fig. 13. Converted stress data (unit: MPa; 6.895 MPa=1ksi) for weld toe in groove-weld segment (Qxy Corresponds to stress shear component. Depth unit is mm; abscissa is Y-distance from flange edge (mm; beam centerline is 76.8mm)

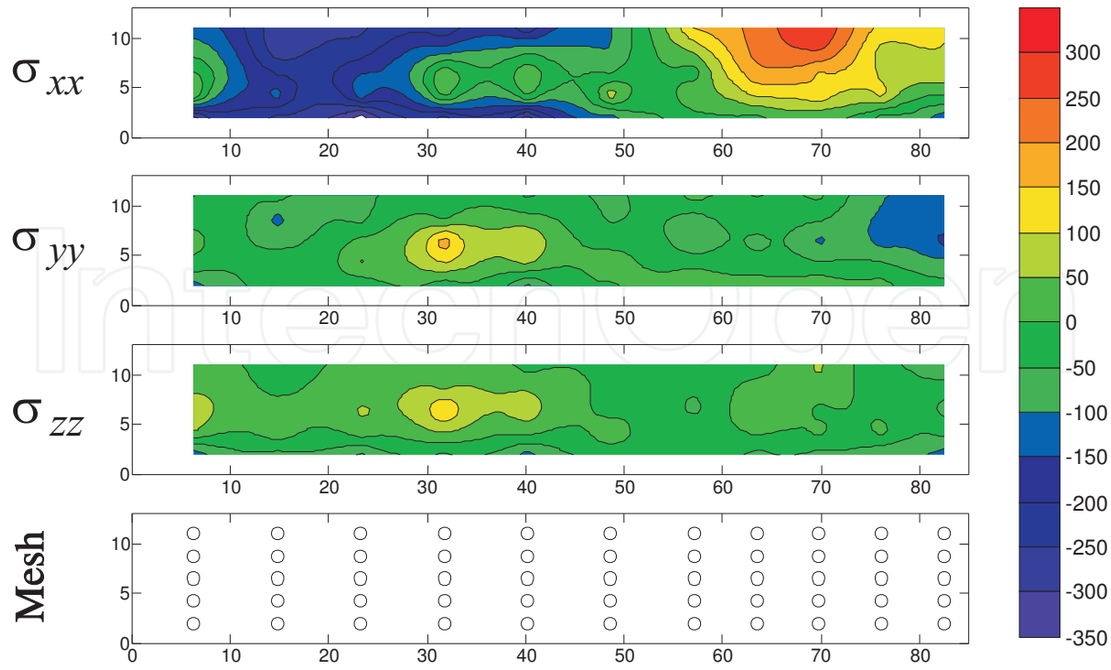

Fig. 14. Contour plots of stress data in Figure 13 for weld toe (MPa; 6.895 MPa=1ksi)

groove weld. Appropriate corrections were made for the measurement points at nominal depth of 2mm based on the FWHM (full-width at half-maximum) values that were used as an indicator of metal differences (base or weld). Relevant details are available elsewhere [NIST, 2003]. The converted stresses in Figure 13 are the data after the corrections. Since the values of d_0 were not obtained directly from the segment itself but from small pieces of corresponding materials (base metal or weld metal) in a similar weld detail, they were given as a range (the upper and lower bounds) for the uncertainty due to the slight material difference and counting statistics in neutron diffraction measurements. Therefore, the values of stresses were also presented as a range which is actually larger than the individual stress-value uncertainties. For the points at nominal depth of Z=2 mm (near outer surface), upper and lower bounds presenting the stress data range are shown as error bars. For the stresses at points on the outer surface near the flange tip (Z=2mm, Y=6.3 mm) where more weld metal was included, the range (difference between the maximum and the minimum values) was greater than other points. Other measurment points in Figure 13 are the average stresses of the maximum and minimum values.

As fatigue stress in the fatigue-tested beams was in the X-direction (longitudinal direction in I-beams), X-direction residual stresses are of the greatest interest. The distributions of near-surface X- stresses along the groove weld bead were re-plotted in Figure 15 for the weld metal, groove weld toe and base metal, respectively. These stress distributions are at nominal depth of about 1.5 to 2mm beneath the outer and inner flange plate surfaces (nominal Z=2 mm and Z=11 mm). Examination of these distributions show that residual stresses near the inner surface (web side) were high in tension near the flange-web connection and high in compression near the flange tip. The stress distribution pattern was similar to the residual stress distribution for longitudinal web-to-flange weld detail [Cheng et al. 2003a], but rather complex since the flanges and web were welded into an I-beam by

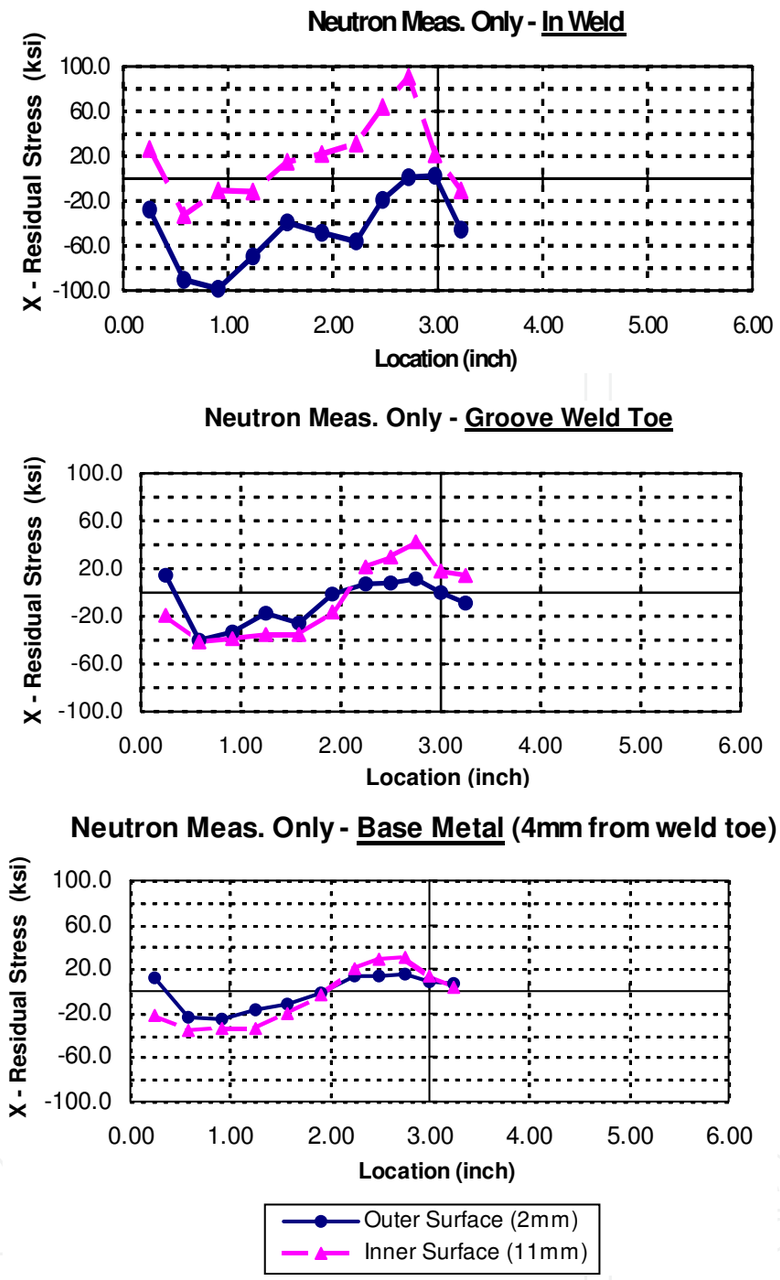

Fig. 15. X-direction stress distributions in groove welded beam (1 in.=25.4 mm; 1 ksi=6.895 MPa; abscissa is Y-distance from flange edge (beam centerline is 76.8mm (~3″))

longitudinal welds after the flange groove weld was completed. Weld residual stresses self-adjusted when single members were assembled into an I-beam to maintain self-equilibrium. The tensile stress near the inner surface reached about 90.6 ksi (625 MPa) in the weld, 42.5 ksi (293 MPa) at the weld toe and 31.3 ksi (216 MPa) in the base metal. These residual stresses in the weld and at the weld toe exceeded or were close to the nominal yield stress, 48~56 ksi, of AL-6XN steel. In fatigue tests, some fatigue cracks have developed from the interior region of the groove weld at the intersection of transverse groove weld and

longitudinal fillet weld, as well as at the weld toe, as shown in Figure 16. On the other hand, residual stresses on outer subsurface (free surface side) are primarily in compression. The magnitudes of the maximum compressive stresses were -98.4 ksi (-679 MPa) in the weld and –40.1 ksi (-277 MPa) at the weld toe, and were comparable to the tensile residual stresses on the inner subsurface. In general, the magnitude of residual stresses decreased when the location was away from the groove weld centerline.

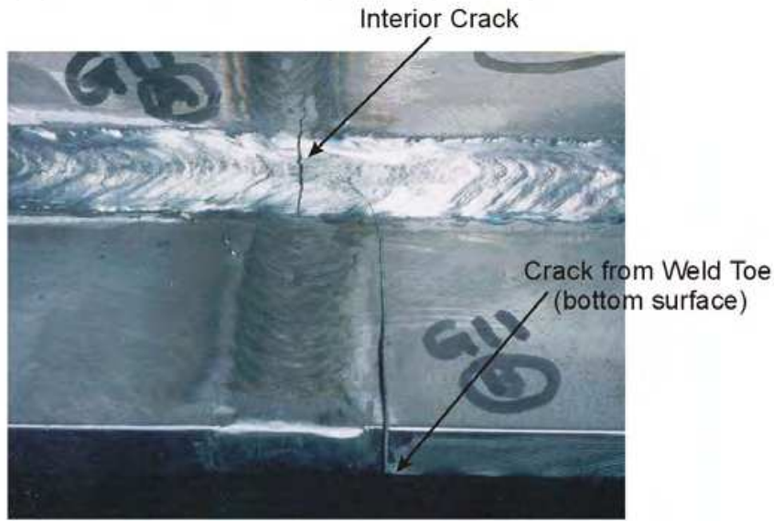

Fig. 16. Typical fatigue cracks from groove weld in AL-6XN beam

It is noted that the data across Section 3 (base metal) and Section 2 (plane at the weld toe, mainly base metal) were of better quality because of the stable conditions in d_0 and d measurements, and fairly good balance was obtained in X-direction equilibrium. For weld metal, grain size variability had an impact on the d_0 measurement due to the much larger grain size than base metal and the irregularity of grain size/micro-structural orientation in the weld material, which caused a d_0 and d incompatibility in calculating strain. Therefore the data scatter for weld material was much larger than for base metal.

6. Results from neutron diffraction measurements for attachment segment

6.1 Measurement locations

Residual Stresses in the attachment-weld segment were also determined by neutron diffraction. The relevant details regarding the use of neutron diffraction were the same as described earilier for the groove-welded segment.

The weld detail studied was an attachment fillet weld between the attachment and the beam flange located near the middle of the segment. Measurements were carried out in a plane along weld toe (A-A Plane in Figure 4) and a plane 7.1 mm away from the weld toe where the strain gages for segment saw cut were located (B′-B′ Plane in Figure 4). Figure 17(a) shows a photo of the attachment weld area. The mesh mapping the nominal measurement points for both A-A and B′-B′ planes is shown in Figure 17(b). The mesh spacing in the Y-direction parallel to fillet weld bead was the same as the strain gage spacing for the segment saw cut.

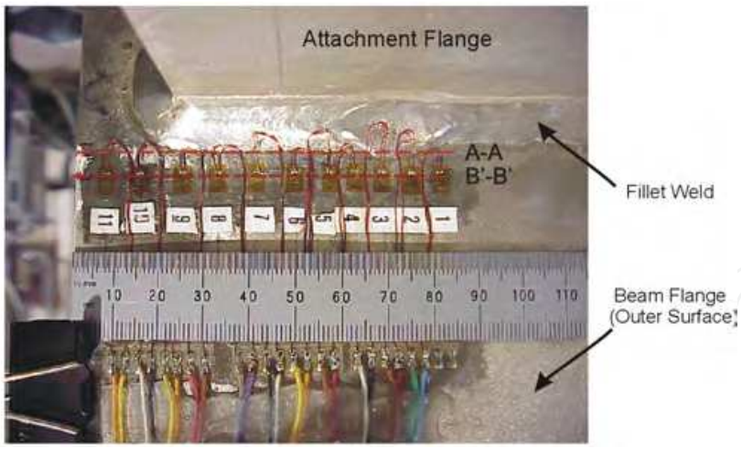

(a)

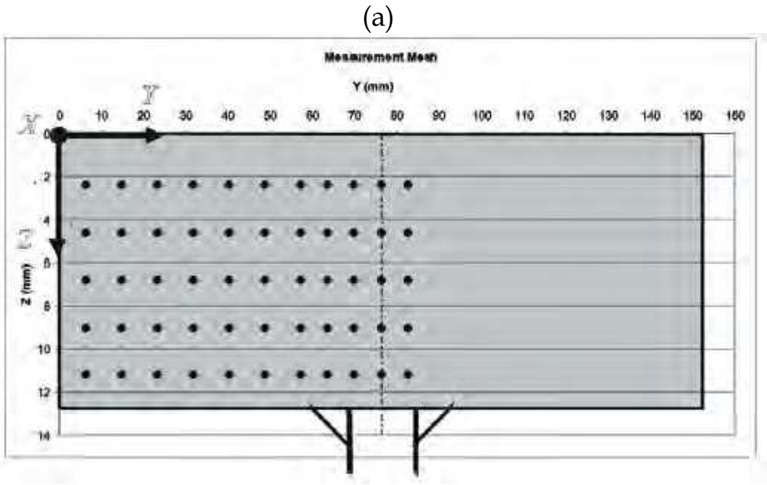

(b)

Fig. 17. Attachment welded beam segment measurement: (a)Close-up view of fillet weld for attachment welded segment; A-A plane at weld toe and B′-B′ plane at 7.1 mm away from weld toe. (b) Complete measurement mesh for beam flange planes at weld toe (A-A) and 7.1 mm away from weld toe (B′-B′). Beam web centerline is at 76.2 mm (3 inch; 1 inch =25.4 mm)

6.2 Measurement results

Figures 18(a) shows the measurement results of the 3-D stresses in the A-A plane (along the weld toe). Both X-stresses (longitudinal direction) and Y-stresses (transverse direction) in the A-A plane near the beam centerline were very high near the outer surface, whereas Z-stresses (depth direction) were very low. The magnitude of the tensile residual stresses in the X-direction was 324 MPa (47.0 ksi) at a nominal depth of 2.4mm and 405 MPa (58.7 ksi) at 4.6 mm, which exceeded the nominal yield stress of AL-6XN steel (48~56 ksi). The maximum tensile stresses in Y-direction were 406 MPa (58.8 ksi) at 2.4 mm depth and 466 MPa (67.5 ksi) at 4.6 mm depth, both of which also exceeded the nominal yield stress. The measurement results for both X-stresses and Y-stresses of the A-A plane, that the stress magnitude was lower at d=2.4 mm than at d=4.6 mm, were not expected. The highest residual tensile stresses were found near the intersection of attachment flange and attachment web welds.

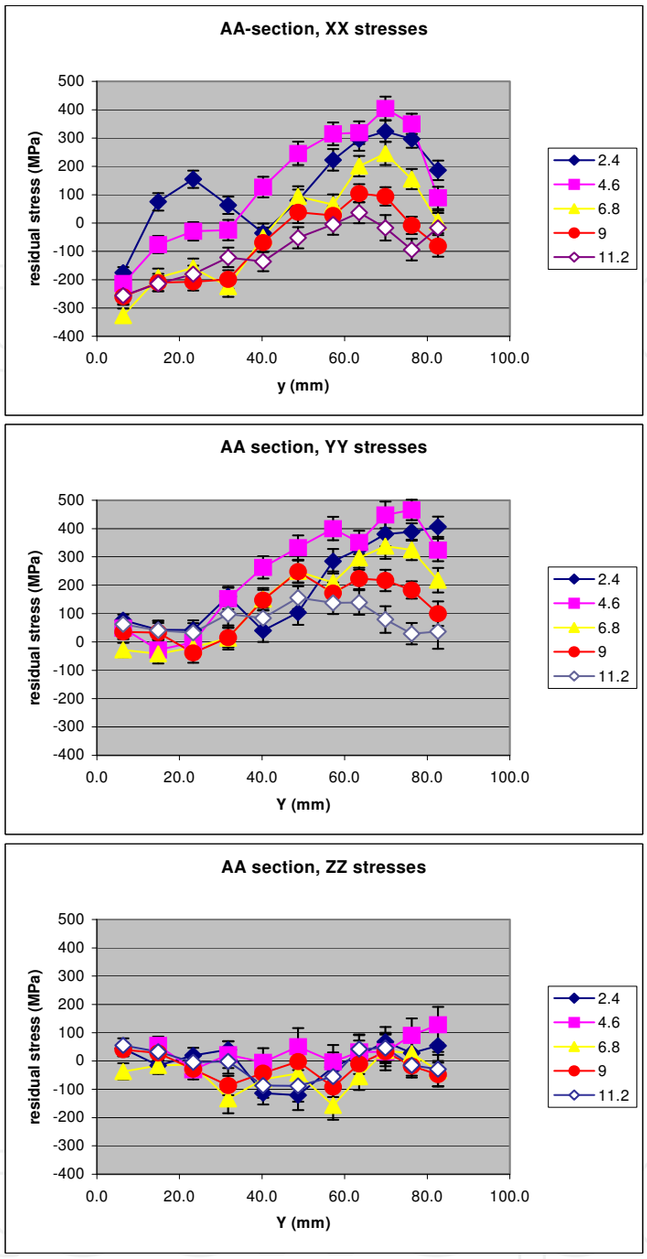

Fig. 18(a). 3-D stress data in A-A plane (weld toe) in attachment weld segment (1 ksi=6.895 MPa; beam centerline at 76.2 mm (1 inch=25.4mm))

Figure 18(b) shows the measurement results of the 3-D stresses in B′-B′ plane (7.1 mm away from A-A) for base metal. The stresses for the B′-B′ plane were less. Further, the dip in stress magnitude with Z=2.4 mm was not seen in the B′-B′ plane. The dip was probably the result of either weld metal or HAZ (heat affected zone) metal being present in the gage volume for $30\text{mm} \leq Y \leq 60\text{mm}$ in the scan length along the weld toe, and was manifested in the raw data by peak widths which were clearly larger than other peak widths for the A-A plane and all of the B′-B′ plane peak widths. In the absence of sufficient data to make a reliable

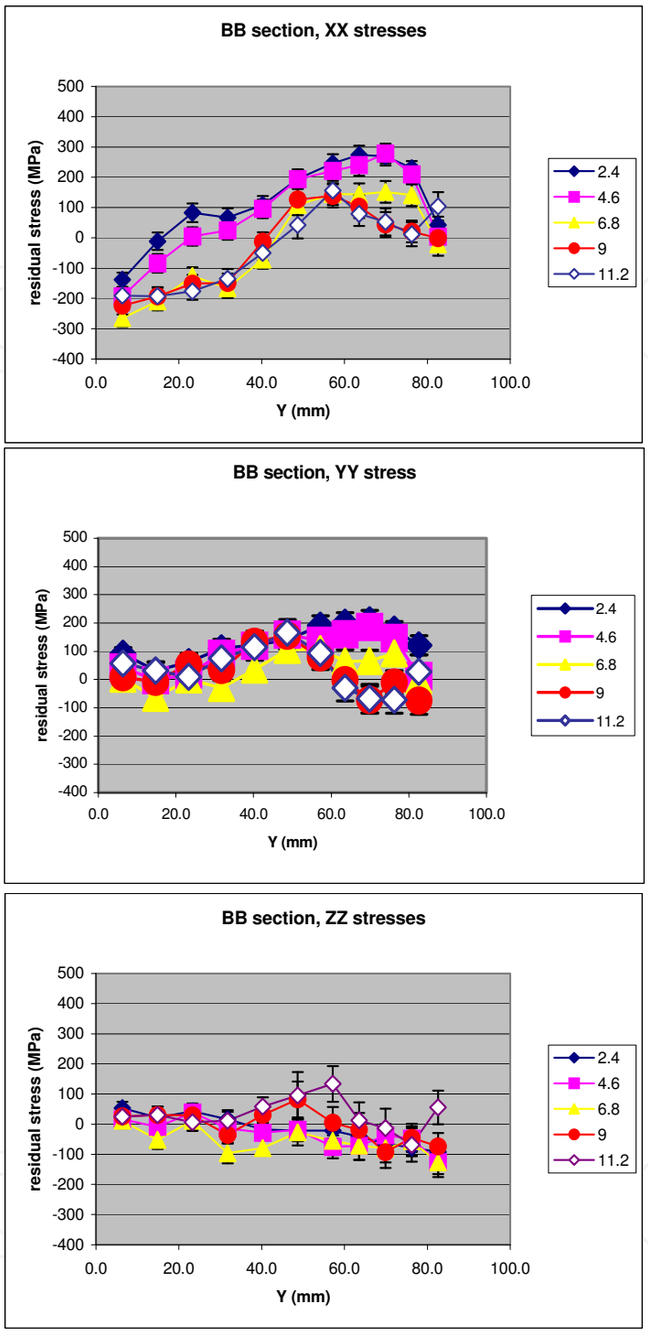

Fig. 18(b). 3-D stress data in B′-B′ plane (base metal) in attachment weld segment (1 ksi=6.895 MPa; beam centerline at 76.2 mm (1 inch=25.4mm))

quantitative correction, it is estimated that X-stresses and Y-stresses of the A-A plane at 2.4 mm should be about equal to the values at 4.6 mm over the scan range, $30\text{mm} \leq Y \leq 80\text{mm}$. The highest residual tensile stresses were near the intersection of attachment flange and attachment web welds. During welding the shrinkage was greater in transverse direction (Y-Y) than in longitudinal direction (X-X).

Residual stresses decayed from outer surface at Z=0, where the attachment was welded, to inner surface. The X-X residual stresses near inner surface (Z=11.2 mm) near the I-beam flange-web welds were much lower than expected. The flange-web welds of the I-beam were expected to produce high tensile residual stresses at the beam flange inner surface, particularly in X-direction. The attachment welds were made on the beam flange after the I-beam was fabricated, and thus a stress re-distribution in the I-beam flange was expected. Residual stresses decayed rapidly away from the weld toe, particularly for stresses in transverse direction (Y-Y).

There was a wrap-around weld at the end of attachment flange. An increase in the longitudinal (X-X) stress was seen near the outer surface (Z=2.4 mm) for both A-A and B'-B' planes. Similar behavior was not observed for the transverse (Y-Y) stress. In general, higher residual tensile stresses near a weld toe were observed parallel to the weld direction rather than perpendicular to the weld direction.

Figure 19 shows the distribution of X-direction residual stresses (the fatigue stress direction) near the outer surface (Z=2.4mm) and the inner surface (Z=11.2mm) of the beam flange for

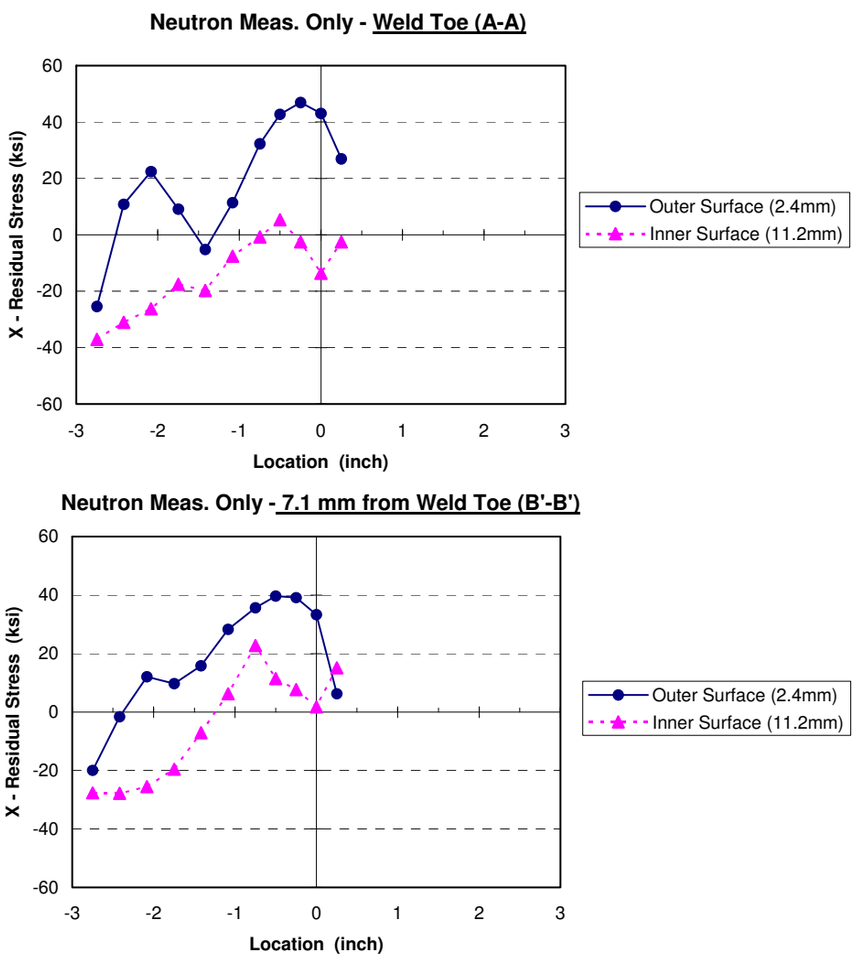

Fig. 19. X-direction stress distribution in attachment weld segment (1 ksi=6.895 MPa; beam centerline at 76.2 mm (1 inch=25.4mm))

A-A (weld toe) and B'-B' (base metal) planes, respectively. These stresses were an average over the 3x3x3 mm cube gage volume measurements. It shows that residual stresses near the outer surface (attachment side) were in tension except near the beam flange tip, and highest near the beam flange-web intersection. The stress was 47 ksi (324 MPa) from neutron diffraction measurement, close to the nominal yield stress of AL-6XN steel. During the fatigue testing program on welded beams with attachments, fatigue cracks were always observed to initiate from the middle of the attachment fillet weld where residual stress was high and from weld start/stop locations. Figure 20 shows a photo of typical fatigue crack that develops under tensile total stress conditions.

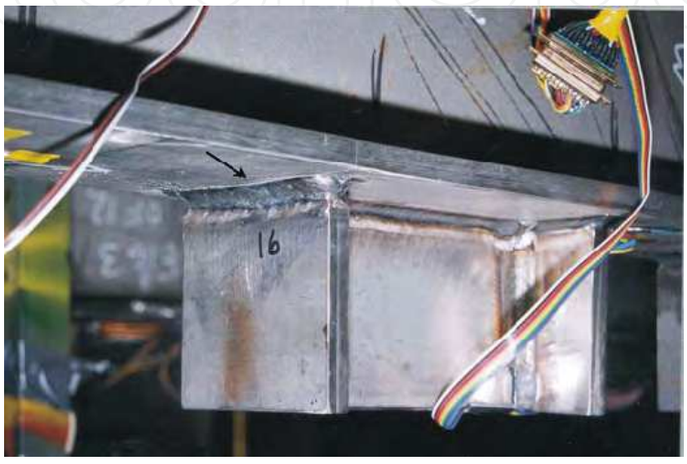

Fig. 20. Typical fatigue crack from attachment fillet weld toe in AL-6XN beam

7. Summary

The objective of this study was to quantify the magnitude and distribution of residual stresses from two types of welded details in AL-6XN steel beams. Residual stresses were measured through destructive saw cutting, and non-destructive neutron diffraction. This chapter showed the measurement results of neutron diffraction. The effect of residual stresses on fatigue strength was discussed. The findings can be summarized as follows.

1. Neutron diffraction method is an effective and powerful tool to measure residual stresses, especially when through-thickness stress distribution and three dimensional stresses are of interest. For large-scale specimens, two measurement methods can be used, such as combination of saw cutting and neutron diffraction as used in this study.
2. Each residual stress measurement technique had advantages and limitations for large scale specimen measurements. The neutron diffraction method provided through-thickness measurements due to its much stronger penetration capacity, and an average measurement within a gage volume normally in ~3x3x3 mm^3 throughout the specimen. It required careful material calibration and it is difficult for the weld metal due to the large grain size. This study showed a good accuracy of neutron diffraction measurements for residual stresses.
3. This study revealed that a large scale welded member has very high tensile residual stresses near weldments, equal to the uniaxial yield stress of the base metal and sometimes even more. Residual stresses decay away from the weld. The attachment-

weld detail exhibited relatively complex distributions along the weld toe and through the flange thickness.

4. Separating a part from a large scale welded assembly provides a partial residual stress release. Such a stress release should not be overlooked when residual stresses are evaluated at a section.

8. Acknowledgment

This study was part of the project on Non-Magnetic Stainless Steel Advanced Double Hall Ships Investigation: Fatigue Resistance of Large Welded Components, supported by the Office of Naval Research (ONR) and directed by Dr. Roshdy G. S. Barsoum, Program Manager. Special thanks are due Dr. Barsoum and his colleauges for their consistent support and help during the entire project. The authors acknowledge the help from the technical staff and fellow workers for the lab work conducted at Fritz Lab and ATLSS Research Center, Lehigh University.

9. Disclaimer

Certain commercial firms and trade names are identified in this report in order to specify aspects of the experimental procedure adequately. Such identification is not intended to imply recommendation or endorsement by the National Institute of Standards and Technology, nor is it intended to imply that the materials or equipment identified are necessarily the best available for the purpose.

10. References

Campus, F. (1954). Effect of Residual Stresses on the Behavior of Structures, *Residual Stress in Metals and Metal Constructions*, William R. Osgood Ed., Prepared for the Ship Structure Committee, Reinhold Publishing Corporation, NY

Cheng, Xiaohua; Fisher, John W.; Prask, Henry J.; Gnaeupel-Herold, Thomas & Luzin, Vladimir (May 2003a). Residual Stress Measurements in AL-6XN Stainless Steel Welded Beams. ATLSS Report No.03-08 (Lehigh University File No. 533612), ONR Grant No. N00014-99-1-0887, Nonmagnetic Stainless Steel for Double Hull Ship Construction, Bethelehem, PA, USA

Cheng, Xiaohua; Fisher, John W.; Prask, Henry J.; Gnaeupel-Herold, Thomas; Yen, Ben T. & Roy, Sougata (2003b). Residual Stress Modification by Post-weld Treatment and Its Beneficial Effect on Fatigue Strength of Welded Structures, *International Journal of Fatigue*, Vol. 25, pp.1219-1269

Danilkin, S.A., Fuess, S., Wieder, T., Hoser, A. (2001). Phonon Dispersion and Elastic Constants in Fe-Cr-Mn-Ni Austenitic Steel, *J. of Materials Science* 36, pp.811-814

Dudt, Philip J. (April 2000). Distortion Control for Stainless Steel Hull Fabrication. NSWCCD-67-TR-2000/07, April, 2000

Fisher, John W.; Yen, Ben T.; Cheng, Xiaohua; Kaufmann, Eric J.; Metrovich, Brian & Ma, Zuozhang (May 2001). Fatigue Resistance of Large Welded AL-6XN Stainless Steel Components with Fillet, Groove, and Attachment Welds, Final Report, Project B, FY 99, ONR Grant No. N00014-99-0887, Nonmagnetic Stainless Steel for Double

Hull Ship Construction, ATLSS Report No.01-04, ATLSS Engineering Research Center, Lehigh University, Bethlehem, PA, USA

HYTEC, Inc. (2001). PRISM System Residual Stress Measurement., www.hytecinc.com

International Association of Classification Society (IACS) (July 1999). No.56 Fatigue Assessment of Ship Structures, *IACS Recom. 56.1*, United Kingdom

The International Nickel Company, Inc. (INCO) (1964). Properties of Some Metals and Alloys, A-297

Lamb, Stephen (Technical Editor) (1999). CASTI Handbook of Stainless Steels & Nickel Alloys, *CASTI Handbook Series*, Vol. 2, CASTI Publishing Inc., Canada

Lu, Le-Wu; Ricles, James M.; Therdphithakvanij, Pholdej; Jang, Seokkwon & Chung, Jin-Oh (Oct. 2002). Compressive Strength of AL-6XN Stainless Steel Plates and Box Columns, Final Report, Project C, FY 99, ONR Grant No. N00014-99-0887, Nonmagnetic Stainless Steel for Double Hull Ship Construction, ATLSS Report No.02-04, ATLSS Research Center, Lehigh University, Bethlehem, PA, USA

NATO ASI Series (1992). Measurement of Residual and Applied Stress Using Neutron Diffraction, Edited by Michael T. Hutchings and Aaron D. Krawitz, *Series E: Applied Sciences*, Vol. 216, (Proceedings of the NATO Advanced Research Workshop on Measurement of Residual and Applied Stress Using Neutron Diffraction, Oxford, UK, March 18-22, 1991,) Kluwer Academic Publishers, Dordrecht, Boston and London

NIST Center for Neutron Research website, www.ncnr.nist.gov, 2011

NIST Center for Neutron Research (2003). The Neutron Diffraction Determination of Residual Stresses in AL-6XN I-Beams, by V. Luzin, T. Gnaeupel-Herold, H. Prask, X. Cheng and J. W. Fisher, NIST internal report

Prask, H. J. & Brand, P. C. (1996). Neutron Diffraction Residual Stress Measurement at NIST, *Material Science Forum*, Vols. 210-213, pp.155-162, Transtec Publications, Switzerland

Prask, Henry J., Gnaupel-Herold, Thomas, Fisher, John W. & Cheng, Xiaohua (June 2001). Residual Stress Modification by Means of Ultrasonic Impact Treatment, *Proc. of Society for Experimental Mechanics Meeting*, Portland, pp. 551-4

Ritchie, D. & Leggatt, R. H. (May 1987). The Measurement of the Distribution of Residual Stresses Through the Thickness of A Welded Joint, *Strain,* Vol. 23, pp. 61-70

Rolled Alloys (April 1997). AL-6XN® Alloy Physical, Mechanical and Corrosion Properties, Technology Department

Sherman, Donald R (April 1969). Residual Stress Measurement in Tubular Members*, Journal of the Structural Division*, Proc. of the ASCE, Vol.95, No.ST4

Society for Experimental Mechanics (SEM), Inc (US) (1996). Handbook of Measurement of Residual Stresses, Edited by Dr. Jian Lu, The Fairmont Press, Inc.

Tebedge, Negussie (1969). Measurement of Residual Stresses – A Study of Methods, MS thesis to Department of Civil Engineering, Lehigh University

Tebedge, N., Alpsten, G. & Tall, L. (Feb 1973). Residual Stress Measurement by Sectioning Method, *Experimental Mechanics*, Vol. 13, No.2, pp. 88-96

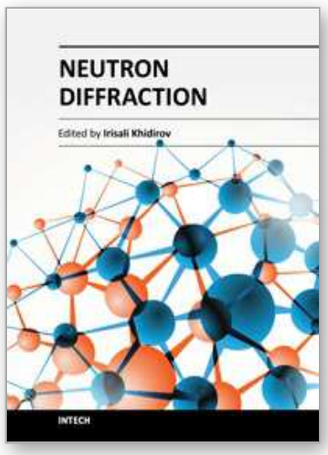

Neutron Diffraction

Edited by Prof. Irisali Khidirov

ISBN 978-953-51-0307-3
Hard cover, 286 pages
Publisher InTech
Published online 14, March, 2012
Published in print edition March, 2012

Now neutron diffraction is widely applied for the research of crystal, magnetic structure and internal stress of crystalline materials of various classes, including nanocrystalls. In the present book, we make practically short excursion to modern state of neutron diffraction researches of crystal materials of various classes. The book contains a helpful information on a modern state of neutron diffraction researches of crystals for the broad specialists interested in studying crystals and purposeful regulation of their service characteristics, since the crystal structure, basically, defines their physical and mechanical properties. Some chapters of the book have methodical character that can be useful to scientists, interested in possibilities of neutron diffraction. We hope, that results of last years presented in the book, can be a push to new ideas in studying of crystalline, magnetic structure and a macrostructure of usual crystal materials and nanocrystals. In turn, it can promote working out of new materials with new improved service characteristics and to origin of innovative ideas.

How to reference

In order to correctly reference this scholarly work, feel free to copy and paste the following:

Xiaohua Cheng, Henry J. Prask, Thomas Gnaeupel-Herold, Vladimir Luzin and John W. Fisher (2012). Neutron Diffraction Measurements for Residual Stresses in AL-6XN Stainless Steel Welded Beams, Neutron Diffraction, Prof. Irisali Khidirov (Ed.), ISBN: 978-953-51-0307-3, InTech, Available from: http://www.intechopen.com/books/neutron-diffraction/neutron-diffraction-measurements-for-residual-stresses-in-al-6xn-stainless-steel-welded-beams

INTECH
open science | open minds

InTech Europe
University Campus STeP Ri
Slavka Krautzeka 83/A
51000 Rijeka, Croatia
Phone: +385 (51) 770 447
Fax: +385 (51) 686 166
www.intechopen.com

InTech China
Unit 405, Office Block, Hotel Equatorial Shanghai
No.65, Yan An Road (West), Shanghai, 200040, China
中国上海市延安西路65号上海国际贵都大饭店办公楼405单元
Phone: +86-21-62489820
Fax: +86-21-62489821

IntechOpen